doi:10.1093/brain/awz039 BRAIN 2019: 142; 1108–1120 | 1108

BRAIN
A JOURNAL OF NEUROLOGY

Cerebral perfusion changes in presymptomatic genetic frontotemporal dementia: a GENFI study

Henri J.M.M. Mutsaerts,[1,*] Saira S. Mirza,[1,*] Jan Petr,[2] David L. Thomas,[3] David M. Cash,[3] Martina Bocchetta,[3] Enrico de Vita,[3] Arron W.S. Metcalfe,[1] Zahra Shirzadi,[1] Andrew D. Robertson,[1] Maria Carmela Tartaglia,[4,5,6] Sara B. Mitchell,[1,6,7] Sandra E. Black,[1,6,7] Morris Freedman,[6,8] David Tang-Wai,[5,6] Ron Keren,[5] Ekaterina Rogaeva,[4] John van Swieten,[9] Robert Laforce Jr,[10] Fabrizio Tagliavini,[11] Barbara Borroni,[12] Daniela Galimberti,[13] James B. Rowe,[14] Caroline Graff,[15] Giovanni B. Frisoni,[16] Elizabeth Finger,[17] Sandro Sorbi,[18] Alexandre de Mendonça,[19] Jonathan D. Rohrer,[3] Bradley J. MacIntosh[1] and Mario Masellis[1,6,7,20] on behalf of the GENetic Frontotemporal dementia Initiative (GENFI)[†]

[*]These authors contributed equally to this work.
[†]Appendix 1.

Genetic forms of frontotemporal dementia are most commonly due to mutations in three genes, *C9orf72*, *GRN* or *MAPT*, with presymptomatic carriers from families representing those at risk. While cerebral blood flow shows differences between frontotemporal dementia and other forms of dementia, there is limited evidence of its utility in presymptomatic stages of frontotemporal dementia. This study aimed to delineate the cerebral blood flow signature of presymptomatic, genetic frontotemporal dementia using a voxel-based approach. In the multicentre GENetic Frontotemporal dementia Initiative (GENFI) study, we investigated cross-sectional differences in arterial spin labelling MRI-based cerebral blood flow between presymptomatic *C9orf72*, *GRN* or *MAPT* mutation carriers ($n = 107$) and non-carriers ($n = 113$), using general linear mixed-effects models and voxel-based analyses. Cerebral blood flow within regions of interest derived from this model was then explored to identify differences between individual gene carrier groups and to estimate a timeframe for the expression of these differences. The voxel-based analysis revealed a significant inverse association between cerebral blood flow and the expected age of symptom onset in carriers, but not non-carriers. Regions included the bilateral insulae/orbitofrontal cortices, anterior cingulate/paracingulate gyri, and inferior parietal cortices, as well as the left middle temporal gyrus. For all bilateral regions, associations were greater on the right side. After correction for partial volume effects in a region of interest analysis, the results were found to be largely driven by the *C9orf72* genetic subgroup. These cerebral blood flow differences first appeared approximately 12.5 years before the expected symptom onset determined on an individual basis. Cerebral blood flow was lower in presymptomatic mutation carriers closer to and beyond their expected age of symptom onset in key frontotemporal dementia signature regions. These results suggest that arterial spin labelling MRI may be a promising non-invasive imaging biomarker for the presymptomatic stages of genetic frontotemporal dementia.

1 Hurvitz Brain Sciences Program, Sunnybrook Research Institute, University of Toronto, Toronto, Canada
2 PET Center, Institute of Radiopharmaceutical Cancer Research, Helmholtz-Zentrum Dresden-Rossendorf, Dresden, Germany
3 Institute of Neurology, University College London, London, UK
4 Tanz Centre for Research in Neurodegenerative Diseases, University of Toronto, Toronto, Canada

Received October 14, 2018. Revised December 14, 2018. Accepted January 4, 2019. Advance Access publication March 7, 2019

5 Memory Clinic, University Health Network, Toronto, Canada
6 Division of Neurology, Department of Medicine, Sunnybrook Health Sciences Centre, University of Toronto, Toronto, Canada
7 L.C. Campbell Cognitive Neurology Research Unit, Sunnybrook Health Sciences Centre, Toronto, Canada
8 Baycrest Centre for Geriatric Care, Toronto, Canada
9 Department of Neurology, Erasmus Medical Center, Rotterdam, The Netherlands
10 Clinique Interdisciplinaire de Mémoire (CIME), Département des Sciences Neurologiques, CHU de Québec, Faculté de médecine, Université Laval, Québec, Canada
11 Fondazione Istituto di Ricovero e Cura a Carattere Scientifico, Milan, Italy
12 Department of Medical and Experimental Sciences, University of Brescia, Brescia, Italy
13 Centro Dino Ferrari, Fondazione Ca' Granda IRCCS Ospedale Policlinico, University of Milan, Milan, Italy
14 Department of Clinical Neurosciences, University of Cambridge, Cambridge, UK
15 Department of Geriatric Medicine, Karolinska Institutet, Stockholm, Sweden
16 IRCCS San Giovanni di Dio Fatebenefratelli, Brescia, Italy
17 Department of Clinical Neurological Sciences, University of Western Ontario, London, Canada
18 Department of Neuroscience, Psychology, Drug Research and Child Health, University of Florence, Florence, Italy
19 Neurology Department, Faculty of Medicine of Lisbon, Portugal
20 Cognitive and Movement Disorders Clinic, Sunnybrook Health Sciences Centre, Toronto, Canada

Correspondence to: Mario Masellis, MSc, MD, PhD
Cognitive and Movement Disorders Clinic, Sunnybrook Health Sciences Centre
2075 Bayview Avenue, Room A4 55
Toronto, Ontario, Canada M4N 3M5
E-mail: mario.masellis@sunnybrook.ca

Keywords: genetic frontotemporal dementia; arterial spin labelling; cerebral blood flow; presymptomatic biomarker

Abbreviations: ASL = arterial spin labelling; GENFI = GENetic Frontotemporal dementia Initiative

Introduction

Frontotemporal dementia encompasses a pathologically heterogeneous group of neurodegenerative diseases, characterized clinically by prominent behavioural and/or language disruption. Frontotemporal dementia significantly impacts patients and their families during the prime of their lives when individuals have responsibilities to their careers, raising children and social interactions (Neary *et al.*, 2005; Onyike and Diehl-Schmid, 2013). It is highly heritable, with an autosomal dominant family history documented in about one-third of people with the disease (Rohrer *et al.*, 2009). Several mutations across three genes (*C9orf72*, *GRN* and *MAPT*) make up the majority of genetic frontotemporal dementia (Seelaar *et al.*, 2011*b*; Warren *et al.*, 2013). The study of presymptomatic mutation carriers compared to non-carriers affords a unique opportunity to understand more about the natural history of genetic frontotemporal dementia during the preclinical phases.

One priority in frontotemporal dementia research is to develop imaging biomarkers (Neary *et al.*, 2005; Rohrer *et al.*, 2013). It is hoped that such biomarkers of genetic frontotemporal dementia could identify those at highest risk of transitioning into the clinical phase, the clinical subtype that will develop, and the age when symptoms will appear. Furthermore, these biomarkers may allow for longitudinal monitoring of disease progression, as well as evaluating efficacy of potential disease-modifying drugs (Cenik *et al.*, 2011; Bateman *et al.*, 2012). Indeed, brain changes have been demonstrated with imaging in presymptomatic/early stage genetic Alzheimer's disease (Bateman *et al.*, 2012). Our structural MRI work on presymptomatic/early stage genetic frontotemporal dementia, as well as that of others, has previously shown early brain changes, particularly in the fronto-insular-temporal regions (Rohrer *et al.*, 2015; Lee *et al.*, 2017; Bertrand *et al.*, 2018). A potential functional imaging biomarker is arterial spin labelling (ASL) perfusion MRI. Increasing evidence suggests that perfusion changes in frontotemporal dementia may be more extensive than structural brain changes early on in the disease course (Olm *et al.*, 2016). ASL allows non-invasive imaging of cerebral blood flow *in vivo* (Alsop *et al.*, 2015). In contrast to other perfusion imaging techniques, ASL uses blood water as an endogenous tracer, which is safe and ideal for longitudinal imaging (Alsop *et al.*, 2015).

Several studies have shown that ASL cerebral blood flow can distinguish symptomatic frontotemporal dementia cases from controls and other dementias (Hu *et al.*, 2010; Shimizu *et al.*, 2010; Binnewijzend *et al.*, 2014; Olm *et al.*, 2016; Steketee *et al.*, 2016). To our knowledge, only one study conducted at a single site has examined the use of ASL perfusion MRI in contrasting presymptomatic *MAPT* and *GRN* mutation carriers ($n = 34$ combined) to non-carriers ($n = 31$) (Dopper *et al.*, 2016). Whilst they did not find any cross-sectional differences in perfusion between carriers and non-carriers at baseline, they demonstrated a significant reduction in perfusion of the frontal pole, superior frontal gyrus, paracingulate gyrus, posterior (mid)cingulate gyrus, precuneus, and thalamus among *GRN* carriers compared to non-carriers on 2

year follow-up scans (Dopper *et al.*, 2016). Furthermore, a significant longitudinal decline in perfusion was observed in frontal, temporal, parietal, and subcortical regions (Dopper *et al.*, 2016). Whilst the results are interesting, they may be unduly limited by the sample size, did not include a robust correction for partial volume effects, and the fact that they did not account for relatedness of the participants in their study design. Herein, we extend on this initial work by investigating the ASL cerebral blood flow signature of presymptomatic frontotemporal dementia in unaffected at-risk family members ($n = 107$ mutation carriers versus $n = 113$ mutation negative controls) participating in the multicentre GENetic Frontotemporal dementia Initiative (GENFI). The aims of this study were: (i) to delineate the cerebral blood flow signature of presymptomatic, genetic frontotemporal dementia using a voxel-based analysis; (ii) to evaluate the effects of genetic subgroup on the regional cerebral blood flow signature; and (iii) to estimate the chronological time frame when presymptomatic changes are observed. We hypothesized an inverse association between perfusion and age, irrespective of mutation carrier status. Furthermore, we posit that the strength of this association will be more prominent in the presymptomatic carriers than in non-carriers and will more strongly relate to their estimated age of expected symptom onset than age alone.

Materials and methods

Participants

Data were drawn from the second data freeze of GENFI (Rohrer *et al.*, 2015), which consisted of centres in the UK, Italy, The Netherlands, Sweden, Portugal and Canada. GENFI participants included known symptomatic carriers of a pathogenic mutation in *C9orf72*, *GRN* or *MAPT* and their first-degree relatives who were at risk of carrying a mutation, but who did not show any symptoms (that is, presymptomatic). Non-carriers were first-degree relatives of symptomatic carriers who did not carry the mutation. The inclusion and exclusion criteria are described in detail elsewhere (Rohrer *et al.*, 2015). As part of the standard GENFI protocol, subjects and a close contact of them were interviewed by a neurologist using a checklist of symptoms relating to frontotemporal dementia. Symptoms were rated as absent, questionable/very mild, mild, moderate or severe in nature and ratings were corroborated by both the patient and their close contact. Presymptomatic individuals scored for the most part as having symptoms absent and, on occasion, in the very mild/questionable range. They also could not have any cognitive, behavioural or language deficits that resulted in a functional decline in terms of both their basic and/or instrumental activities of daily living. Ethical review boards from participating centres approved the GENFI protocol and all participants provided written informed consent according to the Declaration of Helsinki. Data were collected between January 2012 and March 2015 at nine GENFI sites and based on acquiring 3 T ASL and T_1-weighted MRI images in 294 participants. Symptomatic carriers (32 individuals) were excluded from the primary analysis (see statistical analysis section below) since the focus of this study was on the presymptomatic stage. However, as outlined below, perfusion data from symptomatic carriers were included in a secondary analysis. Our semi-automatic quality control procedure (outlined below) excluded 42 scans due to motion and other artefacts. Data from 220 presymptomatic participants were included in the primary analysis (Table 1 and Supplementary Fig. 1).

Table 1 Descriptive characteristics ($n = 220$)

Demographics	Non-carriers ($n = 113$, 51.4%)	Presymptomatic mutation carriers ($n = 107$, 48.6%)	Test statistic
Age (years)	50.1 ± 14.3	46.1 ± 11.5	$t(218) = 2.24$, $P = 0.03$
Sex (male)	41 (36.3%)	41 (38.3%)	$\chi^2(1) = 0.09$, $P = 0.76$
Handedness (right dominant)	103 (91.2%)	96 (89.7%)	$\chi^2(1) = 0.13$, $P = 0.72$
Education (years)	14.1 ± 3.1	14.2 ± 3.0	$t(218) = 0.22$, $P = 0.83$
Average years from expected symptom onset	−9.3 ± 14.4	−11.0 ± 11.8	$t(218) = 0.92$, $P = 0.36$
Carrier status based on genetic subgroup			
C9orf72	34 (30.1%)	34 (31.8%)	$\chi^2(1) = 0.07$, $P = 0.79$
GRN	68 (60.2%)	55 (51.4%)	$\chi^2(1) = 1.72$, $P = 0.19$
MAPT	11 (9.7%)	18 (16.8%)	$\chi^2(1) = 2.41$, $P = 0.12$
Cognitive and behavioural measures			
Mini-Mental State Examination (/30)	29.2 ± 1.1	29.1 ± 1.4	$t(197) = 0.91$, $P = 0.36$
Cambridge Behavioural Inventory-Revised (/180)	3.9 ± 5.7	4.8 ± 10.1	$t(193) = 0.74$, $P = 0.46$
Frontotemporal Dementia Rating Scale (categories[a])	0 (IQR 0–0)	0 (IQR 0–0)	–

Data are *n* (%) or mean ± standard deviation. Statistics for differences between non-carriers and presymptomatic mutation carriers are shown in the fourth column.
IQR = interquartile range.

[a]Frontotemporal Dementia Rating Scale categories = 0 (very mild), 1 (mild), 2 (moderate), 3 (severe), 4 (very severe), and 5 (profound); this scale was designed to be used in symptomatic subjects and so there is a floor effect when applied to presymptomatic subjects leading them to be classified in the very mild range even though they do not have significant functional involvement.

Mutation testing

DNA extraction took place at local sites according to their standard procedures. Mutation testing of participants also took place at local sites either through direct DNA sequencing or allele-specific PCR-based screening of *GRN* or *MAPT*. *C9orf72* hexanucleotide repeat expansions were evaluated using a two-step genotyping procedure as previously described (Dejesus-Hernandez *et al.*, 2011). A pathogenic expansion of *C9orf72* was considered as having more than 30 repeats.

Image acquisition

T_1-weighted and ASL acquisition sequences were harmonized across scanners from different sites, as best as possible (Rohrer *et al.*, 2015). The product ASL sequences are fundamentally different between vendors, thus we opted for four implementations to achieve best results: pseudo-continuous ASL (PCASL) 3D fast-spin-echo stack-of-spirals implemented on a 3 T General Electric MR750 (one site, $n = 22$); PCASL 2D gradient-echo echo-planar imaging (EPI) on a 3 T Philips Achieva, with (one site, $n = 99$) and without (two sites, $n = 32$) background suppression; and a pulsed ASL 3D gradient-and-spin-echo (GRASE) on 3 T Siemens Trio systems (five sites, $n = 67$). ASL parameters are described elsewhere (Mutsaerts *et al.*, 2018).

ASL image processing

We used *ExploreASL* to process the multicentre ASL data (Mutsaerts *et al.*, 2015), a toolbox based on Matlab (MathWorks, MA, USA), Statistical Parametric Mapping 12 (SPM12, Wellcome Trust Centre for Neuroimaging, University College London, UK) and Diffeomorphic Anatomical Registration analysis using Exponentiated Lie algebra (DARTEL) (Ashburner, 2007).

GENFI ASL image processing was optimized to process data from multiple sites, vendors and sequences (Mutsaerts *et al.*, 2018). Briefly, enhanced tissue priors (Lorio *et al.*, 2016) were used to segment the baseline T_1-weighted images into grey and white matter tissue probability maps, which were used to create a population-based DARTEL template (Ashburner, 2007; Stonnington *et al.*, 2008). Motion correction was performed for ASL datasets using a 3D rigid-body transformation with threshold-free motion outlier exclusion based on a threshold-free optimization of the median grey matter voxel-wise temporal signal-to-noise ratio (Wang *et al.*, 2008; Shirzadi *et al.*, 2015). The M0 images were masked and smoothed, and cerebral blood flow was quantified using a single compartment quantification model (Alsop *et al.*, 2015). The cerebral blood flow images were registered to the grey matter image (Mutsaerts *et al.*, 2018). Temporal standard deviation images were used to visually inspect for artefacts that required data filtering (performed by H.J.M.M.M.) (Viviani *et al.*, 2009).

ASL images were reviewed in a two-step procedure. First, vascular regions with negative signal were identified by selecting clusters whose mean cerebral blood flow was below a threshold that was defined as four times the median absolute difference below the median. These voxels were clustered if they were contiguous negative cerebral blood flow values. The signal intensities within the cluster were then sign flipped. Subsequently, voxels with extremely large values were identified by thresholding the cerebral blood flow image at $>80\%$ sorted intensities. This upper threshold was based on a value of four times the median absolute difference above the median. To reduce the influence of these high macrovascular values, while retaining some physiological variability, all values on the cerebral blood flow image above this threshold were non-linearly rescaled (i.e. compressed) rather than hard-clipped. The total number of adapted negative and positive perfusion voxels in our sample was only a small proportion of the whole brain mask, i.e. $4.5 \pm 3.4\%$.

ASL quality control

For inclusion of scans, a novel semi-automatic quality control method was used (Supplementary Fig. 2). This method ranks scans by their spatial coefficient of variation (CoV) (Mutsaerts *et al.*, 2017), which reflects the amount of arterial transit time artefacts. After excluding the worst quality scans (unusable) by visual assessment, all remaining scans were categorized into: (i) 'good' (CoV $\leqslant 0.6$, cerebral blood flow signal predominates

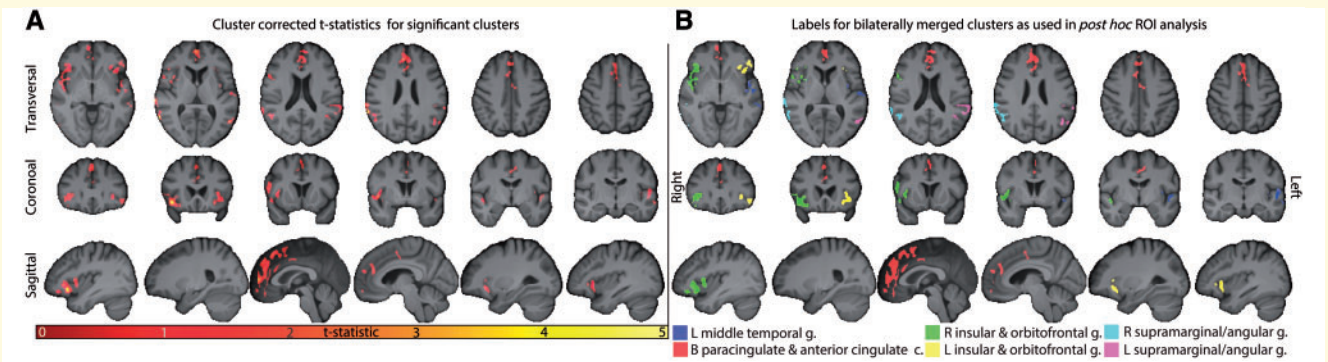

Figure 1 Statistical parametric maps derived from voxel-based mixed effects linear regression model examining the interaction effect between presymptomatic mutation status (carrier versus non-carrier) and years to age of expected symptom onset. Significant clusters were defined using a $P < 0.005$ primary threshold and a $P < 0.05$ FWE cluster-forming threshold (cluster-size = 225 voxels). Both the *t*-statistic maps (**A**) and anatomical labels for clusters used in the *post hoc* region of interest analysis (**B**) are shown. Images are shown in radiological space, overlaid on the mean population 3D T_1-weighted image. c = cortex; g = gyrus; ROI = region of interest.

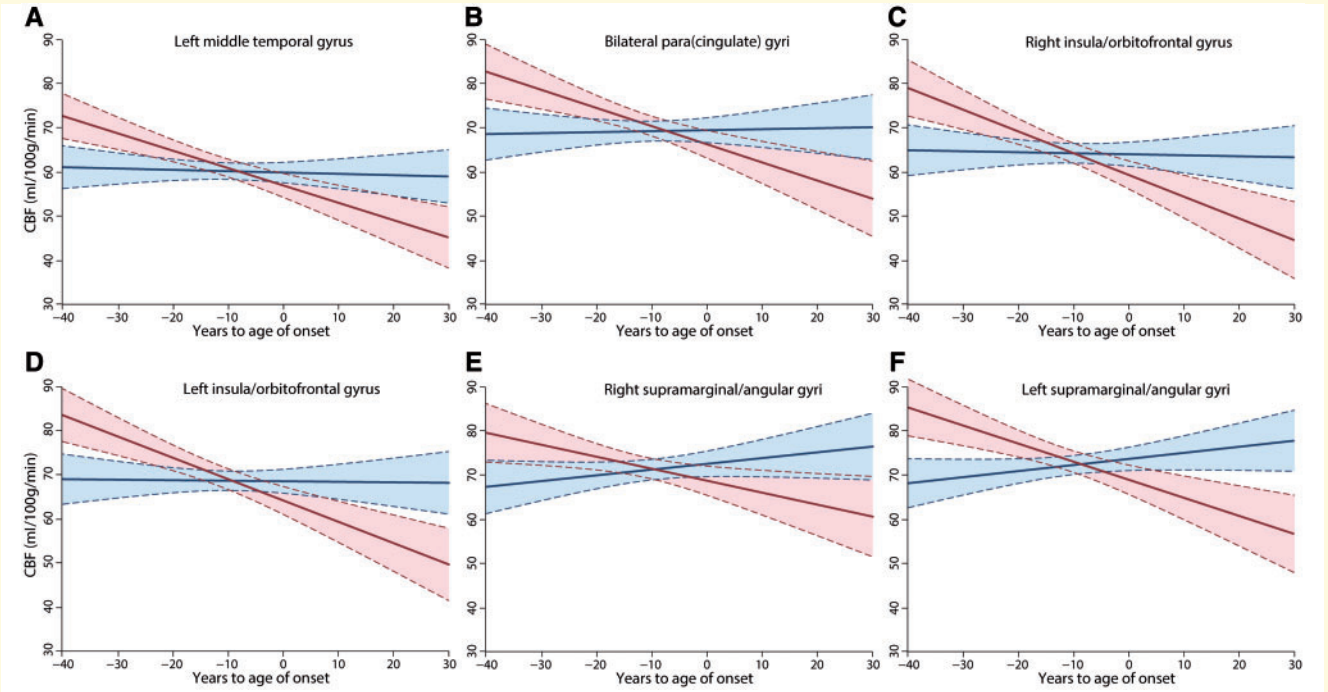

Figure 2 Linear mixed effects model regression lines for each of the six regions of interest plotting cerebral blood flow based on years to age of expected symptom onset in presymptomatic mutation carriers (red) and non-carriers (blue). Shaded areas represent the 95% confidence intervals.

artefacts); (ii) 'acceptable' ($0.6 \leqslant CoV \leqslant 0.8$, both cerebral blood flow signal and artefacts visible); or (iii) 'bad' ($CoV > 0.8$, artefacts predominate cerebral blood flow signal). Three authors (Z.S., A.D.R. and H.J.M.M.M.), each with 3–6 years of experience in handling ASL data, independently reviewed and corrected the CoV-based categorization of the images. Inconsistencies were resolved by consensus. Only the 220 'good' scans were included in the primary analyses (Supplementary Fig. 2).

To adjust for site differences, we performed a spatially varying intensity normalization, which uses the within-site cerebral blood flow similarity between participants to remove the between-site quantification differences. To facilitate this intensity normalization, scanners that contributed <5 artefact-free scans were excluded in the quality control step (nine scans in total).

Residual site effects were minimized by spatial intensity normalization using site-specific bias-fields, as follows: (i) a mean cerebral blood flow image was created for each site; (ii) this image was smoothed with a 6.4 mm full-width at half-maximum (FWHM) Gaussian kernel, constrained by a Montreal Neurological Institute (MNI) brain mask; (iii) these site-specific smoothed mean cerebral blood flow images were averaged to create a population-average cerebral blood flow image, which was rescaled to a mean grey matter cerebral blood flow of 60 ml/100 g/min; (iv) site-specific bias-fields were created by dividing the population-average cerebral blood flow image with the site-specific cerebral blood flow image; and (v) individual cerebral blood flow images were multiplied by site-specific bias field maps.

The voxel-based analysis was restricted to voxels that had both adequate ASL signal-to-noise ratio (Viviani *et al.*, 2009) and were segmented as grey matter with probability $>20\%$.

Statistical analysis

We compared demographic and clinical characteristics between presymptomatic mutation carriers and non-carriers using *t*-tests for continuous and chi-square tests for categorical variables. In our primary analyses, we used linear mixed-effects models to test for cerebral blood flow differences between presymptomatic non-carriers and mutation carriers in voxel-based and regional analyses. This model accounted for fixed and random effects of predictor variables, including intercept terms (Sullivan *et al.*, 1999; Rohrer *et al.*, 2015; Masellis *et al.*, 2016). The fixed effect predictor variables of interest were mutation carrier status, years to age of expected symptom onset, and the interaction between mutation carrier status and years to age of expected symptom onset. Years to age of expected symptom onset was calculated from the mean age at onset in symptomatic family members—e.g. someone aged 50 years at the time of assessment with a mean age at symptom onset of 55 years in their family would have a years to age of expected symptom onset of –5 years (Rohrer *et al.*, 2015). Family membership was included in the model as a random effect, as it was expected that members from the same family might have covariance in brain perfusion due to a shared genetic and environmental background (Rohrer *et al.*, 2015). Sex and site were also added as fixed effect covariates. Age was included as a covariate in a preliminary model but was removed through a model building step because it was captured almost entirely by the years to age of expected symptom onset variable. In a sensitivity analysis, the described model was also run replacing years to age of expected symptom onset with age. The covariance matrix of family relatedness,

stratified by study site, is shown in Supplementary Fig. 1. All analyses on the demographic, clinical, and regional perfusion data were carried out using the Stata Software Version 14.1 (StataCorp, College Station, TX, USA).

Voxel-based analysis and subsequent derivation of regions of interest

The regions where cerebral blood flow was significantly different between presymptomatic carriers and non-carriers were identified from the voxel-based analysis. Images were smoothed, constrained by the voxel-based mask, with a 3.4 mm FWHM Gaussian kernel (Dopper *et al.*, 2016). The primary cluster-forming threshold was $P = 0.005$, with the extent threshold set at $P = 0.05$ for family-wise error (FWE) correction. Regions of lower perfusion identified in the voxel-based analysis in presymptomatic carriers compared to non-carriers based on their years to age of expected symptom onset were named according to their overlap with the Harvard-Oxford atlas (Desikan *et al.*, 2006). These voxel-based identified areas defined our regions of interest. Median grey matter cerebral blood flow was extracted from each region of interest for subsequent regional analyses within the overall group, as well as stratified between genetic subgroups. The region of interest analyses evaluated whether there were differences in the associations linking extracted cerebral blood flow with years to age of expected symptom onset between presymptomatic carriers and non-carriers using linear mixed models, taking into account fixed effects of sex and site, and random effects of family membership as covariates. To test if there were non-linear changes in cerebral blood flow, we also tested a quadratic term for years to age of expected symptom onset. Sensitivity analyses were performed by repeating the analysis with age replacing years to age of expected symptom onset and after a high-only winsorization of 0 to 10 values of cerebral blood flow to account for cerebral blood flow outliers.

Partial volume correction

We implemented a partial volume correction to mitigate any regional tissue differences that would act as a confound (Asllani *et al.*, 2008). Region of interest analyses were performed with and without the partial volume correction. Since the regions of interest were derived from the voxel-based analysis, which was restricted to the grey matter, they were dilated centrally to include sufficient white matter voxels for a robust partial volume correction. Specifically, the region of interest was eroded in volume until the white matter voxels accounted for $<50\%$ of the total volume. As a result of differences in effective resolution and smoothness between ASL sites (Mutsaerts *et al.*, 2018), we estimated the effective spatial resolution based on the different ASL implementations (Vidorreta *et al.*, 2013; Mutsaerts *et al.*, 2018), which could contribute to partial volume error. We assumed the following effective resolutions in FWHM: $3.7 \times 3.7 \times 7.6$ mm (2D EPI with background suppression), $4.6 \times 4.6 \times 4.3$ mm (2D EPI without background suppression), $3.75 \times 3.75 \times 5.5$ mm (3D GRASE) (Vidorreta *et al.*, 2013), $5.0 \times 5.0 \times 9.5$ mm (3D spiral).

Timing of cerebral blood flow decline

Instead of stratifying years to age of expected symptom onset at regular time points, e.g. 5- or 10-year intervals, we used a quantile approach to account for the high physiological cerebral blood flow variability on an individual basis by ensuring equal numbers of participants per time interval. Subsequently, the association between quantiles of years to age of expected symptom onset and cerebral blood flow was tested using linear mixed models, adjusting for sex and site (fixed effects), and family (random effects) as covariates in presymptomatic non-carriers and carriers separately. In these models, the quantile variable was used as a categorical predictor variable with the first quantile as the reference quantile. We tested quintiles, sextiles, septiles, octiles, and deciles to ensure robustness of results. Since octiles enabled us to explore smaller intervals with a reasonable number of participants per interval to obtain valid estimates, we present results for octiles only.

Secondary analysis comparing symptomatic and presymptomatic mutation carriers

To understand the perfusion data further, we compared cerebral blood flow in mutation carriers who were symptomatic ($n = 31$) to those who remained presymptomatic past their expected age of symptom onset ($n = 23$). This was done using *t*-tests and linear regression models adjusted for age and sex of participants. This analysis used cerebral blood flow that was extracted from within the voxel-based defined regions of interest as described previously. As we were interested in comparing cerebral blood flow in symptomatic versus presymptomatic carriers who were beyond their expected age of symptom onset, we excluded all non-carriers, presymptomatic carriers who did not meet this criterion, and one symptomatic mutation carrier who had a very high cerebral blood flow value in the left supramarginal/angular gyri, thus considered an outlier.

Data availability

Data will be shared according to the GENFI data sharing agreement, after review by the GENFI data access committee with final approval granted by the GENFI steering committee.

Results

Demographic, cognitive and behavioural measures and family distribution across sites

Apart from mutation carriers being younger than non-carriers, no significant differences in demographic, general cognitive and behavioural measures were observed between the two groups (Table 1). Supplementary Fig. 1 provides an overview of the family distribution across the different sites for all participants. Site and family membership were strongly related, but nonetheless were considered as covariates due to the importance of both of these factors.

Table 2 Anatomical localization of voxel-based analysis-derived clusters of cerebral blood flow

Cluster	Cluster size (ml)	Peak *t*-score	Peak MNI coordinates (mm)		
			x	*y*	*z*
L middle temporal gyrus	4.2	4.4	−60.0	−33.0	−1.5
B anterior cingulate/paracingulate gyri	12.8	4.6	+9.0	+54.0	−9.0
R anterior insula, orbitofrontal gyri	7.8	5.2	+42.0	+22.5	−10.5
L anterior insula, orbitofrontal gyri	2.6	4.3	−30.0	+25.5	−7.5
R supramarginal/angular gyri	4.0	5.9	+63.0	−55.5	+6.0
L supramarginal/angular gyri	2.8	4.6	−52.5	−63.0	+9.0

Clusters for the cerebral blood flow interaction between age to expected symptom onset and mutation carrier status, for primary cluster-forming threshold $P = 0.005$ and FWE threshold $P = 0.05$. B = bilateral; L = left; R = right.

Voxel-based analysis

Years to age of expected symptom onset predicted a lower cerebral blood flow due to decline in perfusion with age. While no main effect of carrier status on cerebral blood flow was observed, we identified a robust and statistically significant carrier status × years to age of expected symptom onset interaction. Specifically, as shown by Table 2 and Fig. 1, we identified several regions with a significantly greater inverse association between cerebral blood flow and the expected age of symptom onset in presymptomatic mutation carriers compared to non-carriers. Six regions were identified by the voxel-based analysis including: the left middle temporal gyrus, bilateral anterior cingulate/paracingulate gyri, bilateral anterior insula/orbitofrontal gyri, and bilateral supramarginal/angular gyri. The peak *t*-statistics were higher for clusters in the right hemisphere compared to the left hemisphere for the anterior insula/orbitofrontal gyri ($t = 5.2$ versus $t = 4.8$), supramarginal/angular gyri ($t = 5.8$ versus $t = 4.6$) and for the anterior cingulate/paracingulate cortex ($t = 4.6$ versus $t = 3.9$).

Regions of interest analysis

Table 3 shows the difference in association of cerebral blood flow with years to age of expected symptom onset between presymptomatic carriers and non-carriers within the voxel-based analysis-defined regions of interest in the overall group and stratified for genetic subgroup, with and without partial volume correction. The main effect of years to age of expected symptom onset and the interaction effect of years to age of expected symptom onset × carrier status were significantly associated with cerebral blood flow in all regions of interest, with the exception of the right supramarginal/angular gyri wherein only the interaction term was significant. These results were consistent before and after partial volume correction in the entire cohort. In analyses without partial volume correction applied, all genetic subgroups contributed to the main effect of years to age of expected symptom onset. However, after partial volume correction was applied, results seemed to be largely driven by the *C9orf72* group. The interaction between years to age of expected symptom onset and carrier status was only found in the *C9orf72* group after applying partial volume correction.

The quadratic term for years to expected age of symptom onset was not significant and did not improve the model fit, therefore, it was not included in the model. In a sensitivity analysis, when years to age of expected symptom onset was replaced by age, the same clusters survived, albeit to a lesser extent. The regional analysis was also repeated with age instead of years to age of expected symptom onset and after high-only winsorization of zero to 10 values to account for cerebral blood flow outliers, which did not change the results.

Estimation of time of cerebral blood flow decline

In the analyses of octiles of years to age of expected symptom onset and cerebral blood flow in the entire cohort, we observed that cerebral blood flow in carriers started to differ significantly from the fourth octile onward (corresponding to −14.8 to −9.3 years) compared to the first octile, which was used as a reference (−40.9 to −25.1 years). This means that on average, the change in cerebral blood flow in presymptomatic carriers starts to occur at ∼12.5 years before their expected years to age of symptom onset. This pattern was observed for all regions of interest (Supplementary Tables 1 and 2) in presymptomatic mutation carriers only. No differences in cerebral blood flow between the octiles were observed in non-carriers (Supplementary Tables 1 and 2, and Fig. 2). Figure 2 represents cerebral blood flow decline in presymptomatic carriers and non-carriers over years to age of expected symptom onset in each of the identified voxel-based analysis-defined regions of interest. Carriers who were several years away from their age of predicted symptom onset had higher cerebral blood flow values than non-carriers with similar years to age of expected symptom onset. In contrast, carriers who were beyond their age of expected symptom onset had lower cerebral blood flow values than non-carriers with similar years to age of expected symptom onset. This resulted in a steeper negative slope of the regression lines for each region of interest in carriers than in

Table 3 Region of interest analysis comparing cerebral blood flow between carriers and non-carriers modelled based on years to age of expected symptom onset and its interaction with carrier status

VBA-derived regions of interest	All carriers (*n* = 107) versus non-carriers (*n* = 113)				*C9orf72* carriers (*n* = 34) versus non-carriers (*n* = 113)				*GRN* carriers (*n* = 55) versus non-carriers (*n* = 113)				*MAPT* carriers (*n* = 18) versus non-carriers (*n* = 113)			
	β	CI	*P*	P_{int}	β	CI	*P*	P_{int}	β	CI	*P*	P_{int}	β	CI	*P*	P_{int}
Regions of interest without partial volume correction																
L middle temporal gyrus	−0.20	(−0.32, −0.09)	0.001	<0.001	−0.15	(−0.27, −0.02)	0.026	0.001	−0.05	(−0.18, 0.07)	0.393	0.127	−0.10	(−0.25, 0.05)	0.186	<0.001
B anterior cingulate/paracingulate gyri	−0.38	(−0.53, −0.23)	<0.001	<0.001	−0.29	(−0.46, −0.12)	0.001	<0.001	−0.18	(−0.35, −0.02)	0.027	0.023	−0.20	(−0.38, −0.01)	0.038	0.002
R anterior insula, orbitofrontal gyri	−0.35	(−0.50, −0.20)	<0.001	<0.001	−0.28	(−0.45, −0.11)	0.001	0.001	−0.17	(−0.33, −0.01)	0.039	0.042	−0.20	(−0.38, −0.01)	0.041	0.001
L anterior insula, orbitofrontal gyri	−0.35	(−0.49, −0.21)	<0.001	<0.001	−0.32	(−0.49, −0.16)	<.001	<0.001	−0.19	(−0.35, −0.03)	0.016	0.154	−0.23	(−0.40, −0.06)	0.009	0.007
R supramarginal/angular gyri	−0.06	(−0.21, 0.08)	0.379	<0.001	0.05	(−0.11, 0.20)	0.547	0.004	0.09	(−0.06, 0.24)	0.249	0.002	−0.12	(−0.06, 0.29)	0.187	<0.001
L supramarginal/angular gyri	−0.20	(−0.33, −0.06)	0.004	<0.001	−0.14	(−0.29, 0.01)	0.072	<0.001	−0.02	(−0.16, 0.12)	0.771	0.055	−0.03	(−0.19, 0.14)	0.752	<0.001
Regions of interest with partial volume correction																
L middle temporal gyrus	−0.16	(−0.27, −0.05)	0.005	0.007	−0.15	(−0.28, −0.02)	0.026	0.006	−0.05	(−0.18, 0.07)	0.408	0.248	−0.06	(−0.19, 0.08)	0.420	0.371
B anterior cingulate/paracingulate gyri	−0.15	(−0.28, −0.01)	0.035	0.008	−0.10	(−0.26, −0.05)	0.205	0.024	−0.02	(−0.18, 0.13)	0.769	0.181	−0.01	(−0.18, 0.15)	0.86	0.208
R anterior insula, orbitofrontal gyri	−0.20	(−0.33, −0.07)	0.003	0.003	−0.15	(−0.31, 0.005)	0.057	0.007	−0.07	(−0.22, 0.08)	0.343	0.108	−0.06	(−0.22, −0.10)	0.472	0.151
L anterior insula, orbitofrontal gyri	−0.18	(−0.31, −0.05)	0.007	0.001	−0.16	(−0.31, −0.004)	0.045	0.001	−0.04	(−0.19, 0.10)	0.546	0.171	−0.04	(−0.20, 0.12)	0.604	0.254
R supramarginal/angular gyri	−0.02	(−0.15, 0.12)	0.809	0.021	0.01	(−0.15, 0.18)	0.876	0.025	0.09	(−0.07, 0.24)	0.264	0.227	0.11	(−0.06, 0.28)	0.206	0.373
L supramarginal/angular gyri	−0.07	(−0.20, 0.07)	0.336	0.001	−0.03	(−0.19, −013)	0.728	0.002	0.08	(−0.07, 0.24)	0.304	0.080	0.11	(−0.05, 0.27)	0.196	0.138

Cerebral blood flow difference in carriers versus non-carriers in association with years to age of expected symptom onset, (β, 95% confidence interval, *P*-value, and *P*-value of interaction between carrier-status and years to age of expected symptom onset).

Regions of interest from the voxel-based analysis (VBA) were derived, and were used for mixed effects models with and without partial volume error correction (Asllani *et al.*, 2008). Estimates represent difference in cerebral blood flow between carriers and non-carriers and were adjusted for sex (fixed) and family relatedness (random). *P* represents *P*-values for the association between cerebral blood flow and years to age of expected symptom onset, and P_{int} represents the *P*-value for interaction between gene carrier-status and years to age of expected symptom onset on cerebral blood flow in the particular group. B = bilateral; L = left; R = right.

non-carriers, which remained consistent after we repeated our analyses with mean-centred cerebral blood flow values. A similar pattern of results was observed across all regions of interest.

Secondary analysis comparing symptomatic and presymptomatic mutation carriers

While mean cerebral blood flow values were always lower in symptomatic carriers (demographic characteristics in Supplementary Table 3) than in presymptomatic carriers who were beyond their expected age of symptom onset (Supplementary Table 4), this association only reached statistical significance in the bilateral cingulate and insulae/orbitofrontal gyri, as well as the left supramarginal/angular gyri. Linear regression models also showed similar results after adjusting for age and sex (Supplementary Table 5).

Discussion

This multicentre GENFI ASL perfusion study has identified frontal, temporal and parietal brain regions where cerebral blood flow is altered among presymptomatic frontotemporal dementia mutation carriers compared to non-carrier family members. We found some evidence of a laterality effect, whereby the right hemisphere appeared to be more affected than the left hemisphere in the frontoparietal regions. The specific brain regions detected include: the medial frontal cortex, specifically the bilateral anterior cingulate and paracingulate gyri; the orbitofronto-insular cortex bilaterally; the inferior parietal region, specifically the bilateral supramarginal and angular gyri; and the left middle temporal gyrus. Our important and novel findings are highlighted by the following. First, presymptomatic mutation carriers were slightly younger than non-carriers, further strengthening the premise that the mutations, in combination with expected age at symptom onset, had a greater impact on cerebral perfusion than age alone. Second, adjusting for potential atrophy effects through partial volume correction did not influence the gene carrier to cerebral blood flow associations, but nonetheless seemed to implicate a stronger cerebral blood flow influence for the *C9orf72* carriers compared to the *GRN* and *MAPT* gene carrier subgroups. Third, the lower regional cerebral blood flow in presymptomatic mutation carriers based on age from estimated time of symptom onset occurred approximately 12.5 years before the average age of onset of symptoms in affected family members, albeit from a higher baseline level of cerebral blood flow. In presymptomatic carriers compared to non-carriers, the slight increase in cerebral blood flow seen between octile −9.1 to −4.7 years may represent a rebound phenomenon. It is conceivable that in order to preserve behaviour, cognition and function as an individual approaches their expected age of symptom onset, there may be a compensatory rise in cerebral blood flow before it becomes more severely deficient. Alternatively, this may simply be the result of natural variation in cerebral blood flow and an artefact of the cross-sectional analysis performed here. This phenomenon will be explored in more detail in future longitudinal analyses correlating it with changes in behavioural and cognitive performance. Fourth, in a secondary analysis, presymptomatic carriers who were beyond their expected age of symptom onset had relatively higher regional cerebral blood flow than symptomatic carriers indicating the potential protective effects of preserved cerebral blood flow with respect to delaying symptom onset.

These findings demonstrate the potential utility of non-invasive perfusion MRI as an early imaging biomarker for genetic forms of frontotemporal dementia during the presymptomatic phase. The medial frontal and orbitofronto-insular regions of hypoperfusion identified as presymptomatic carriers approached their expected age of symptom onset in this study overlap with regions of atrophy identified in our previous neuroanatomical study (Cash *et al.*, 2018). These regions are part of a distributed network previously shown to be involved in aberrant socio-emotional processing observed in frontotemporal dementia. Specifically, the anterior insula is a critical hub region that, together with the dorsal anterior cingulate cortex, form part of the salience network and the paralimbic system involved in cognitive, sensory and affective regulation (Menon, 2015). The orbitofrontal cortex receives limbic projections from the cingulate and parahippocampal cortices, hippocampus and amygdala and also receives innervation from all the sensory modalities, thus integrating sensory, memory and emotional information (Viskontas *et al.*, 2007). Anatomically, it transitions into the insula via the frontoinsular cortex, which is an agranular region that contains von Economo neurons (Seeley, 2010). This neuronal cell type is also present in the anterior cingulate cortex further strengthening the cytoarchitectonic link between these two cortical regions (Seeley, 2010).

Accumulating evidence indicates that von Economo neurons may be most susceptible early on to neuropathological and degenerative processes involved in frontotemporal dementia (Seeley *et al.*, 2006), leading some to posit that this cell type is responsible for the early regional vulnerability of the anterior cingulate and insular cortices (Seeley *et al.*, 2007). With respect to clinical phenotype, behavioural variant frontotemporal dementia is nearly four times as common as presentations with primary progressive aphasia (Hogan *et al.*, 2016). The reason for this observation is not known, but the rightward, regional frontal involvement seen in the current study overlaps with findings in studies of symptomatic frontotemporal dementia. Specifically, prior imaging (Miller *et al.*, 1993; Mychack *et al.*, 2001; Schroeter *et al.*, 2007; Gordon *et al.*, 2016) and pathological case series (Irwin *et al.*, 2018) have shown regional involvement of the anterior cingulate/paracingulate, orbitofrontal and/or anterior insular cortices with a right

hemispheric predilection for behavioural variant frontotemporal dementia. Based on our findings in the context of existing literature, we anticipate that the majority of our presymptomatic cohort would be predisposed to develop behavioural variant frontotemporal dementia, which is the subject of future study using longitudinal GENFI data. If the theory of vulnerability via von Economo neurons in early stage frontotemporal dementia is correct, then the right-predominant hemispheric involvement in frontotemporal dementia may be related to the higher number of susceptible von Economo neurons in the right anterior insula and anterior cingulate cortex than on the left in post-natal brains (Allman *et al.*, 2011).

Hypoperfusion was also seen in the left middle temporal gyrus in presymptomatic carriers in relation to their expected age of symptom onset. The posterior aspect of this structure is strongly connected to the left inferior frontal gyrus, and together they contribute to controlled semantic retrieval (Davey *et al.*, 2015). A quantitative meta-analysis has revealed that the semantic variant of primary progressive aphasia is associated with grey matter atrophy involving the bilateral inferior temporal and fusiform gyri, the medial aspect of the temporal lobes (including parahippocampal gyri and amygdala), as well as the left temporal pole, middle temporal gyrus, and caudate (Yang *et al.*, 2012). Whether or not presymptomatic mutation carriers who have prominent hypoperfusion involving the left middle temporal gyrus will go on to develop clinical features of semantic dementia will have to be determined through longitudinal monitoring of the GENFI cohort.

The inferior parietal lobule bilaterally showed lower perfusion in presymptomatic carriers compared to non-carriers in association with their expected age at symptom onset. This structure is made up of the supramarginal (rostral portion) and angular (caudal portion) gyri, and through connections with frontal, temporal and occipital cortex, it is important for sensorimotor integration (Caspers *et al.*, 2013). In the left hemisphere, the inferior parietal lobule is part of the dorsal stream for auditory perception playing a role in verbal working memory, phonological short term memory, and temporal ordering of articulation and sound (Binkofski *et al.*, 2016). It is also involved in motor functions and interactions with objects (Binkofski *et al.*, 2016). The left angular gyrus is involved in reading, writing, verbal repetition, naming, processing of semantic content and contributes to modality-independent conceptual and semantic processes linking language and action networks (Binkofski *et al.*, 2016). In the right hemisphere, the rostral and middle inferior parietal lobule is involved in spatial coding and attention, as well as learning and execution of complex sequential motor movements, including those involved in multi-tool/object use (Binkofski *et al.*, 2016). Bilaterally, the rostral inferior parietal lobule forms part of the ventrodorsal stream of visual perception involved in sensorimotor information processing based on object use representations; lesions to this structure can impair both pantomime and real object use resulting in limb apraxia (Binkofski *et al.*, 2016). On the right side, the angular gyrus is involved in spatial functions with lesions of this structure producing hemi-neglect (Binkofski *et al.*, 2016). There is evidence of atrophy, reduced functional connectivity and perfusion, and pathological involvement of the inferior parietal lobule that correlates with disturbances in language and praxis observed in *GRN*-related frontotemporal dementia (Rohrer *et al.*, 2010; Seelaar *et al.*, 2011*a*; Premi *et al.*, 2014; Kim *et al.*, 2016). Therefore, it is possible that the presymptomatic *GRN* carriers in this study might be driving our observed cerebral blood flow association with the inferior parietal lobule, although we did not have the power to assess this directly.

Interestingly, as illustrated in Fig. 2, presymptomatic mutation carriers tended on average to have higher perfusion than non-carriers several years before their predicted age of symptom onset, but carriers who were beyond their predicted age of symptom onset tended to have lower perfusion than their non-carrier counterparts in the same time period. This raises the possibility that compensatory mechanisms involving cerebral perfusion may be at work early during the presymptomatic phase in mutation carriers to maintain normal brain functions. Compensatory mechanisms have been hypothesized to be at play in young *APOE* ε4 allele carriers at risk for Alzheimer's disease using both resting state and task-based functional MRI demonstrating increased default mode network connectivity at rest and during an encoding task compared to their non-carrier counterparts (Filippini *et al.*, 2009). However, a more recent ASL perfusion MRI study in cognitively normal older adults carrying the *APOE* ε4 allele demonstrated increased perfusion involving the medial frontal cortex, medial and lateral temporal cortex, parietal regions, insula, and the basal ganglia that was associated with worse verbal memory functions (Zlatar *et al.*, 2016). Other than the use of different functional imaging modalities, it is possible that the conflicting observations might be due to differences in the age of the participants included in the two studies. For example, compensatory mechanisms may start to break down in older *APOE* ε4 participants due to increasing age as Alzheimer's brain pathological burden becomes more prominent and we hypothesize a similar process may be seen in autosomal dominant frontotemporal dementia. Data presented in Fig. 2 and Supplementary Table 1 should be interpreted with caution as they do not compare carriers to non-carriers directly. However, both show different cerebral blood flow trajectories in carriers and non-carriers indicating a similar time window of cerebral blood flow decline in carriers in all regions.

Whilst we did not have sufficient statistical power to identify regions of hypoperfusion in mutation carriers stratified by genetic subgroup in independent voxel-based analyses, the *post hoc* regions of interest analysis produced some noteworthy results. Firstly, *C9orf72* and *MAPT* mutation carriers showed the observed inverse association between cerebral blood flow and years to age of expected

symptom onset in all six regions identified from the original combined group analysis, whereas *GRN* mutation carriers only showed this effect in the bilateral anterior cingulate/paracingulate, right anterior insula/orbitofrontal, and right supramarginal/angular gyri. This finding is in line with previous literature demonstrating that *GRN* mutations lead to asymmetric involvement of the brain (Masellis *et al.*, 2006; Gabryelewicz *et al.*, 2010; Rohrer and Warren, 2011), whereas both *MAPT* and *C9orf72*-related frontotemporal dementia tends to present with more symmetrical brain findings (Rohrer and Warren, 2011; Mahoney *et al.*, 2012). Finally, only the *C9orf72* mutation carriers showed persistent perfusion deficits after partial volume correction in all regions of interest. This suggests that early presymptomatic perfusion anomalies in *C9orf72* mutation carriers are robust and not as significantly influenced by underlying structural changes in the same cortical regions. These regional presymptomatic perfusion deficits are consistent with the known slowly progressive behavioural and neuropsychiatric symptoms that occur over many years in *C9orf72* mutation carriers (Khan *et al.*, 2012; Galimberti *et al.*, 2013; Devenney *et al.*, 2014).

Because of the multicentre nature of this study, one of the main strengths is that we were able to acquire the largest ASL sample, to date, of presymptomatic individuals at-risk for genetic frontotemporal dementia. However, one drawback of multicentre ASL studies is variability from MRI vendor and/or sequence acquisition procedures (Alsop *et al.*, 2015). We attempted to mitigate nuisance effects through the use of a robust ASL software package (Mutsaerts *et al.*, 2018), which included partial volume error correction (Mutsaerts *et al.*, 2014), intensity normalization, and semi-automatic quality control (Mutsaerts *et al.*, 2017). This has allowed GENFI to overcome the current status quo in ASL imaging studies of neurodegenerative diseases that restricts analyses to those scanned on the same MRI platform, such as what is done in the Alzheimer's Disease Neuroimaging Initiative (ADNI) and Parkinson's Progression Marker Initiative (PPMI); this significantly limits ASL sample sizes to only a subset of participants in those studies. Another strength is that we included Family as a random factor in our linear mixed-effect models to account for effects of both unknown genomic or environmental influences that may co-vary with cerebral perfusion changes in the participants. Limitations include the relatively small sample size of the genetic subgroups, which reduced power in subgroup analyses. However, through our use of a voxel-based analysis in the entire cohort to identify regions of interest with subsequent *post hoc* analysis restricted to these regions, we have been able to detect some genetic subgroup differences. Another challenge of using the ASL MRI technique is that physiological perfusion fluctuations are high on both an intra- and interindividual basis. For example, diurnal effects, drug effects, and post-prandial state have been shown to influence perfusion (Clement *et al.*, 2017). This may limit the discovery of small neurovascular coupling-related effects to studies with large sample sizes.

Cerebral blood flow was inversely associated with an individual's expected age of symptom onset in presymptomatic mutation carriers compared to non-carriers, in signature regions previously implicated in symptomatic frontotemporal dementia. The regional analyses that applied partial volume correction suggest that these effects were most significant in *C9orf72* hexanucleotide repeat expansion carriers. These results make ASL MRI promising as a non-invasive imaging biomarker for the presymptomatic stages of genetic frontotemporal dementia. Future work will focus on longitudinal analysis, as well as attempting to identify other factors that lead to phenoconversion to symptomatic frontotemporal dementia. Therapeutic strategies that can preserve or improve cerebral blood flow may hold promise in preventing or delaying symptom onset, respectively, in at-risk presymptomatic mutation carriers, or potentially reversing symptoms in early symptomatic stages of frontotemporal dementia.

Acknowledgements

The authors wish to express their gratitude to the participants and their families for taking part in the GENFI study.

Funding

This work was funded by the UK Medical Research Council, the Italian Ministry of Health and the Canadian Institutes of Health Research as part of a Centres of Excellence in Neurodegeneration grant, and also a Canadian Institutes of Health Research operating grant (MOP 327387) and funding from the Weston Brain Institute to M.M. J.D.R. is supported by an MRC Clinician Scientist Fellowship (MR/M008525/1) and has received funding from the NIHR Rare Disease Translational Research Collaboration (BRC149/NS/MH). This work was also supported by the MRC UK GENFI grant (MR/M023664/1). The funders had no role in study design, data collection and analysis, decision to publish, or preparation of the manuscript.

Competing interests

The authors report no competing interests.

Supplementary material

Supplementary material is available at *Brain* online.

Appendix 1

GENFI consortium

Full details are available in the Supplementary material. Christin Andersson, Silvana Archetti, Andrea Arighi,

Luisa Benussi, Giuliano Binetti, Maura Cosseddu, Katrina M. Dick, Marie Fallström, Carlos Ferreira, Chiara Fenoglio, Nick C. Fox, Giorgio Fumagalli, Stefano Gazzina, Roberta Ghidoni, Marina Grisoli, Vesna Jelic, Lize Jiskoot, Gemma Lombardi, Carolina Maruta, Simon Mead, Lieke Meeter, Rick van Minkelen, Benedetta Nacmias, Linn Öijerstedt, Sebastien Ourselin, Alessandro Padovani, Jessica Panman, Michela Pievani, Cristina Polito, Enrico Premi, Sara Prioni, Rosa Rademakers, Veronica Redaelli, Giacomina Rossi, Martin N. Rossor, Elio Scarpini, Hakan Thonberg, Pietro Tiraboschi, Ana Verdelho, Jason D. Warren.

References

Allman JM, Tetreault NA, Hakeem AY, Manaye KF, Semendeferi K, Erwin JM, et al. The von Economo neurons in the frontoinsular and anterior cingulate cortex. Ann N Y Acad Sci 2011; 1225: 59–71.

Alsop DC, Detre JA, Golay X, Gunther M, Hendrikse J, Hernandez-Garcia L, et al. Recommended implementation of arterial spin-labeled perfusion MRI for clinical applications: A consensus of the ISMRM perfusion study group and the European consortium for ASL in dementia. Magn Reson Med 2015; 73: 102–16.

Ashburner J. A fast diffeomorphic image registration algorithm. Neuroimage 2007; 38: 95–113.

Asllani I, Borogovac A, Brown TR. Regression algorithm correcting for partial volume effects in arterial spin labeling MRI. Magn Reson Med 2008; 60: 1362–71.

Bateman RJ, Xiong C, Benzinger TL, Fagan AM, Goate A, Fox NC, et al. Clinical and biomarker changes in dominantly inherited Alzheimer's disease. N Engl J Med 2012; 367: 795–804.

Bertrand A, Wen J, Rinaldi D, Houot M, Sayah S, Camuzat A, et al. Early cognitive, structural, and microstructural changes in presymptomatic c9orf72 carriers younger than 40 years. JAMA Neurol 2018; 75: 236–45.

Binkofski FC, Klann J, Caspers S. On the neuroanatomy and functional role of the inferior parietal lobule and intraparietal sulcus. In: Hick G, Small SL, editors. Neurobiology of language. London, San Diego, Waltham, Oxford: Elsevier; 2016.

Binnewijzend MA, Kuijer JP, van der Flier WM, Benedictus MR, Moller CM, Pijnenburg YA, et al. Distinct perfusion patterns in Alzheimer's disease, frontotemporal dementia and dementia with Lewy bodies. Eur Radiol 2014; 24: 2326–33.

Cash DM, Bocchetta M, Thomas DL, Dick KM, van Swieten JC, Borroni B, et al. Patterns of gray matter atrophy in genetic frontotemporal dementia: results from the GENFI study. Neurobiol Aging 2018; 62: 191–6.

Caspers S, Schleicher A, Bacha-Trams M, Palomero-Gallagher N, Amunts K, Zilles K. Organization of the human inferior parietal lobule based on receptor architectonics. Cereb Cortex 2013; 23: 615–28.

Cenik B, Sephton CF, Dewey CM, Xian X, Wei S, Yu K, et al. Suberoylanilide hydroxamic acid (vorinostat) up-regulates progranulin transcription: rational therapeutic approach to frontotemporal dementia. J Biol Chem 2011; 286: 16101–8.

Clement P, Mutsaerts HJ, Vaclavu L, Ghariq E, Pizzini FB, Smits M, et al. Variability of physiological brain perfusion in healthy subjects—a systematic review of modifiers. Considerations for multi-center ASL studies. J Cereb Blood Flow Metab 2018; 38: 1418–37.

Davey J, Cornelissen PL, Thompson HE, Sonkusare S, Hallam G, Smallwood J, et al. Automatic and controlled semantic retrieval: TMS reveals distinct contributions of posterior middle temporal gyrus and angular gyrus. J Neurosci 2015; 35: 15230–9.

Dejesus-Hernandez M, Mackenzie IR, Boeve BF, Boxer AL, Baker M, Rutherford NJ, et al. Expanded GGGGCC hexanucleotide repeat in noncoding region of C9ORF72 causes chromosome 9p-linked FTD and ALS. Neuron 2011; 72: 245–56.

Desikan RS, Segonne F, Fischl B, Quinn BT, Dickerson BC, Blacker D, et al. An automated labeling system for subdividing the human cerebral cortex on MRI scans into gyral based regions of interest. Neuroimage 2006; 31: 968–80.

Devenney E, Hornberger M, Irish M, Mioshi E, Burrell J, Tan R, et al. Frontotemporal dementia associated with the C9ORF72 mutation: a unique clinical profile. JAMA Neurol 2014; 71: 331–9.

Dopper EG, Chalos V, Ghariq E, den HT, Hafkemeijer A, Jiskoot LC, et al. Cerebral blood flow in presymptomatic MAPT and GRN mutation carriers: a longitudinal arterial spin labeling study. Neuroimage Clin 2016; 12: 460–5.

Filippini N, MacIntosh BJ, Hough MG, Goodwin GM, Frisoni GB, Smith SM, et al. Distinct patterns of brain activity in young carriers of the APOE-epsilon4 allele. Proc Natl Acad Sci USA 2009; 106: 7209–14.

Gabryelewicz T, Masellis M, Berdynski M, Bilbao JM, Rogaeva E, St George-Hyslop P, et al. Intra-familial clinical heterogeneity due to FTLD-U with TDP-43 proteinopathy caused by a novel deletion in progranulin gene (PGRN). J Alzheimers Dis 2010; 22: 1123–33.

Galimberti D, Fenoglio C, Serpente M, Villa C, Bonsi R, Arighi A, et al. Autosomal dominant frontotemporal lobar degeneration due to the C9ORF72 hexanucleotide repeat expansion: late-onset psychotic clinical presentation. Biol Psychiatry 2013; 74: 384–91.

Gordon E, Rohrer JD, Fox NC. Advances in neuroimaging in frontotemporal dementia. J Neurochem 2016; 138 (Suppl 1): 193–210.

Hogan DB, Jette N, Fiest KM, Roberts JI, Pearson D, Smith EE, et al. The prevalence and incidence of frontotemporal dementia: a systematic review. Can J Neurol Sci 2016; 43 (Suppl 1): S96–109.

Hu WT, Wang Z, Lee VM, Trojanowski JQ, Detre JA, Grossman M. Distinct cerebral perfusion patterns in FTLD and AD. Neurology 2010; 75: 881–8.

Irwin DJ, McMillan CT, Xie SX, Rascovsky K, Van Deerlin VM, Coslett HB, et al. Asymmetry of post-mortem neuropathology in behavioural-variant frontotemporal dementia. Brain 2018; 141: 288–301.

Khan BK, Yokoyama JS, Takada LT, Sha SJ, Rutherford NJ, Fong JC, et al. Atypical, slowly progressive behavioural variant frontotemporal dementia associated with C9ORF72 hexanucleotide expansion. J Neurol Neurosurg Psychiatry 2012; 83: 358–64.

Kim G, Ahmadian SS, Peterson M, Parton Z, Memon R, Weintraub S, et al. Asymmetric pathology in primary progressive aphasia with progranulin mutations and TDP inclusions. Neurology 2016; 86: 627–36.

Lee SE, Sias AC, Mandelli ML, Brown JA, Brown AB, Khazenzon AM, et al. Network degeneration and dysfunction in presymptomatic C9ORF72 expansion carriers. Neuroimage Clin 2017; 14: 286–97.

Lorio S, Fresard S, Adaszewski S, Kherif F, Chowdhury R, Frackowiak RS, et al. New tissue priors for improved automated classification of subcortical brain structures on MRI. Neuroimage 2016; 130: 157–66.

Mahoney CJ, Downey LE, Ridgway GR, Beck J, Clegg S, Blair M, et al. Longitudinal neuroimaging and neuropsychological profiles of frontotemporal dementia with C9ORF72 expansions. Alzheimers Res Ther 2012; 4: 41.

Masellis M, Collinson S, Freeman N, Tampakeras M, Levy J, Tchelet A, et al. Dopamine D2 receptor gene variants and response to rasagiline in early Parkinson's disease: a pharmacogenetic study. Brain 2016; 139: 2050–62.

Masellis M, Momeni P, Meschino W, Heffner R Jr, Elder J, Sato C, et al. Novel splicing mutation in the progranulin gene causing familial corticobasal syndrome. Brain 2006; 129: 3115–23.

Menon V. Salience network. In: Toga AW, editor. Brain mapping: an encyclopedic reference. Amsterdam, Boston: Academic Press, Elsevier; 2015. p. 597–611.

Miller BL, Chang L, Mena I, Boone K, Lesser IM. Progressive right frontotemporal degeneration: clinical, neuropsychological and SPECT characteristics. Dementia 1993; 4: 204–13.

Mutsaerts HJ, Petr J, Vaclavu L, van Dalen JW, Robertson AD, Caan MW, et al. The spatial coefficient of variation in arterial spin labeling cerebral blood flow images. J Cereb Blood Flow Metab 2017; 37: 3184–92.

Mutsaerts HJ, Steketee RM, Heijtel DF, Kuijer JP, van Osch MJ, Majoie CB, et al. Inter-vendor reproducibility of pseudo-continuous arterial spin labeling at 3 Tesla. PLoS One 2014; 9: e104108.

Mutsaerts HJ, van Osch MJ, Zelaya FO, Wang DJ, Nordhoy W, Wang Y, et al. Multi-vendor reliability of arterial spin labeling perfusion MRI using a near-identical sequence: implications for multi-center studies. Neuroimage 2015; 113: 143–52.

Mutsaerts HJMM, Petr J, Thomas DL, De VE, Cash DM, van Osch MJP, et al. Comparison of arterial spin labeling registration strategies in the multi-center GENetic frontotemporal dementia initiative (GENFI). J Magn Reson Imaging 2018; 47: 131–40.

Mychack P, Kramer JH, Boone KB, Miller BL. The influence of right frontotemporal dysfunction on social behavior in frontotemporal dementia. Neurology 2001; 56: S11-S15.

Neary D, Snowden J, Mann D. Frontotemporal dementia. Lancet Neurol 2005; 4: 771–80.

Olm CA, Kandel BM, Avants BB, Detre JA, Gee JC, Grossman M, et al. Arterial spin labeling perfusion predicts longitudinal decline in semantic variant primary progressive aphasia. J Neurol 2016; 263: 1927–38.

Onyike CU, Diehl-Schmid J. The epidemiology of frontotemporal dementia. Int Rev Psychiatry 2013; 25: 130–7.

Premi E, Cauda F, Gasparotti R, Diano M, Archetti S, Padovani A, et al. Multimodal FMRI resting-state functional connectivity in granulin mutations: the case of fronto-parietal dementia. PLoS One 2014; 9: e106500.

Rohrer JD, Guerreiro R, Vandrovcova J, Uphill J, Reiman D, Beck J, et al. The heritability and genetics of frontotemporal lobar degeneration. Neurology 2009; 73: 1451–6.

Rohrer JD, Nicholas JM, Cash DM, van SJ, Dopper E, Jiskoot L, et al. Presymptomatic cognitive and neuroanatomical changes in genetic frontotemporal dementia in the Genetic Frontotemporal dementia Initiative (GENFI) study: a cross-sectional analysis. Lancet Neurol 2015; 14: 253–62.

Rohrer JD, Ridgway GR, Modat M, Ourselin S, Mead S, Fox NC, et al. Distinct profiles of brain atrophy in frontotemporal lobar degeneration caused by progranulin and tau mutations. Neuroimage 2010; 53: 1070–6.

Rohrer JD, Warren JD. Phenotypic signatures of genetic frontotemporal dementia. Curr Opin Neurol 2011; 24: 542–9.

Rohrer JD, Warren JD, Fox NC, Rossor MN. Presymptomatic studies in genetic frontotemporal dementia. Rev Neurol (Paris) 2013; 169: 820–4.

Schroeter ML, Raczka K, Neumann J, Yves von CD. Towards a nosology for frontotemporal lobar degenerations-a meta-analysis involving 267 subjects. Neuroimage 2007; 36: 497–510.

Seelaar H, Papma JM, Garraux G, de Koning I, Reijs AE, Valkema R, et al. Brain perfusion patterns in familial frontotemporal lobar degeneration. Neurology 2011a; 77: 384–92.

Seelaar H, Rohrer JD, Pijnenburg YA, Fox NC, van Swieten JC. Clinical, genetic and pathological heterogeneity of frontotemporal dementia: a review. J Neurol Neurosurg Psychiatry 2011b; 82: 476–86.

Seeley WW. Anterior insula degeneration in frontotemporal dementia. Brain Struct Funct 2010; 214: 465–75.

Seeley WW, Allman JM, Carlin DA, Crawford RK, Macedo MN, Greicius MD, et al. Divergent social functioning in behavioral variant frontotemporal dementia and Alzheimer disease: reciprocal networks and neuronal evolution. Alzheimer Dis Assoc Disord 2007; 21: S50–7.

Seeley WW, Carlin DA, Allman JM, Macedo MN, Bush C, Miller BL, et al. Early frontotemporal dementia targets neurons unique to apes and humans. Ann Neurol 2006; 60: 660–7.

Shimizu S, Zhang Y, Laxamana J, Miller BL, Kramer JH, Weiner MW, et al. Concordance and discordance between brain perfusion and atrophy in frontotemporal dementia. Brain Imaging Behav 2010; 4: 46–54.

Shirzadi Z, Crane DE, Robertson AD, Maralani PJ, Aviv RI, Chappell MA, et al. Automated removal of spurious intermediate cerebral blood flow volumes improves image quality among older patients: a clinical arterial spin labeling investigation. J Magn Reson Imaging 2015; 42: 1377–85.

Steketee RM, Bron EE, Meijboom R, Houston GC, Klein S, Mutsaerts HJ, et al. Early-stage differentiation between presenile Alzheimer's disease and frontotemporal dementia using arterial spin labeling MRI. Eur Radiol 2016; 26: 244–53.

Stonnington CM, Tan G, Kloppel S, Chu C, Draganski B, Jack CR Jr, et al. Interpreting scan data acquired from multiple scanners: a study with Alzheimer's disease. Neuroimage 2008; 39: 1180–5.

Sullivan LM, Dukes KA, Losina E. Tutorial in biostatistics. An introduction to hierarchical linear modelling. Stat Med 1999; 18: 855–88.

Vidorreta M, Wang Z, Rodriguez I, Pastor MA, Detre JA, Fernandez-Seara MA. Comparison of 2D and 3D single-shot ASL perfusion fMRI sequences. Neuroimage 2013; 66: 662–71.

Viskontas IV, Possin KL, Miller BL. Symptoms of frontotemporal dementia provide insights into orbitofrontal cortex function and social behavior. Ann N Y Acad Sci 2007; 1121: 528–45.

Viviani R, Sim EJ, Lo H, Richter S, Haffer S, Osterfeld N, et al. Components of variance in brain perfusion and the design of studies of individual differences: the baseline study. Neuroimage 2009; 46: 12–22.

Wang Z, Aguirre GK, Rao H, Wang J, Fernandez-Seara MA, Childress AR, et al. Empirical optimization of ASL data analysis using an ASL data processing toolbox: ASLtbx. Magn Reson Imaging 2008; 26: 261–9.

Warren JD, Rohrer JD, Rossor MN. Clinical review. Frontotemporal dementia. BMJ 2013; 347: f4827.

Yang J, Pan P, Song W, Shang HF. Quantitative meta-analysis of gray matter abnormalities in semantic dementia. J Alzheimers Dis 2012; 31: 827–33.

Zlatar ZZ, Bischoff-Grethe A, Hays CC, Liu TT, Meloy MJ, Rissman RA, et al. Higher brain perfusion may not support memory functions in cognitively normal carriers of the ApoE epsilon4 allele compared to non-carriers. Front Aging Neurosci 2016; 8: 151.